Technique Report | Received 24 April 2026; Revised 6 July 2026; Accepted 18 July 2026; Published 31 July 2026
https://doi.org/10.55092/la20260006

Retarded migration liquid chromatography separation eliminates flow path interferences for ultrasensitive and accurate quantification of DNA N6-methyladenine

Weiyi Lai[1], Meiling Lu[2], Jiezhen Mo[1], Zhilin Hou[1] and Hailin Wang[1,3,4,*]

[1] State Key Laboratory of Environmental Chemistry and Ecotoxicology, Research Center for Eco-Environmental Sciences, Chinese Academy of Sciences, Beijing 100085, China
[2] Greater China Market Division, Agilent Technologies, Beijing 100102, China
[3] University of Chinese Academy of Sciences, Beijing 100049, China
[4] School of Environment, Hangzhou Institute for Advanced Study, University of Chinese Academy of Sciences (UCAS), Hangzhou 310024, China

* Correspondence author; E-mail: hlwang@rcees.ac.cn.

Highlights:

- liquid chromatography (LC) flow path is a hidden source of N6-methyladenine (6mA) contamination in MS analysis.
- Novel migration-retardation strategy eliminates flow path 6mA interference.
- Tandem LC columns physically resolve authentic 6mA from contaminants.
- Achieved ultra-sensitive 6mA quantification limit of 5 amol (signal-to-noise ratio (S/N) ≥ 10).
- Validated in mammalian cells, correcting up to 30-fold overestimation by conventional LC.

Abstract: DNA N6-methyladenine (6mA) modification is widespread in prokaryotes and unicellular eukaryotes but relatively rare in multicellular organisms. Intriguingly, we found that the deoxynucleoside 6mA within the liquid chromatography (LC) flow path and causes overestimation in 6mA content. To identify the rare yet authentic presence of DNA 6mA in mammals and understand its biological functions, it is critical to eliminate the interference flow-path-related 6mA contamination. Here, we designed a flow path 6mA migration-retardation separation approach using two tandem LC columns. By this new design authentic 6mA released from mammalian genomic DNA can be completely resolved from flow-path-related 6mA contamination. Armed with this innovative design, DNA 6mA is detected with a limit of quantification of approximately 5×10^{-18} mol (signal-to-noise ratio (S/N) ≥ 10). Furthermore, the method was validated in complex biological matrices, demonstrating negligible matrix effects and high recovery. Application across 12 mammalian cell lines revealed that conventional single-column LC methods can overestimate 6mA levels by up to 30-fold, whereas our dual-column strategy effectively eliminates this systematic bias for accurate ultra-trace quantification.

Keywords: DNA N6-methyladenine (6mA); ultrahigh-performance liquid chromatography–tandem mass spectrometry (UHPLC-MS/MS); contamination; migration-retardation separation

1. Introduction

DNA N6-methyladenine (6mA) is a DNA modification that has been extensively studied in prokaryotes [1,2] and some eukaryotes, including *Drosophila* [3], *Chlamydomonas* [4], *Tetrahymena* [5], and *Oxytricha* [6]. This modification plays crucial roles in numerous prokaryotic biological processes, such as restriction-modification systems [7], gene expression regulation [8], DNA repair [9], DNA replication [10], and cell cycle control [11]. 6mA is also present at relatively high levels in some lower eukaryotes. For example, it constitutes approximately 0.7% of total adenines in *Tetrahymena* [5], 1.28% in *P. Bursaria* [12], and 0.4% in *Chlamydomona* [4]. In these organisms, 6mA is primarily located within the 5'-ApT-3' motif [4,5,12–14] and exhibits specific genomic distributions. Emerging evidence suggests that 6mA may be involved in diverse biological processes in lower eukaryotes, including chromatin organization, gene expression regulation [14], DNA replication, and transposon silencing.

Additionally, the roles of 6mA in mammalian DNA are garnering increasing attention [11]. The methyltransferase METTL4 might catalyze the methylation of N6-adenine in mitochondrial DNA, which is crucial for regulating the mitochondrial stress response [15,16]. The prokaryotic AlkB homolog ALKBH1 might function as a 6mA demethylase and showed a preference for bubbled or bulged DNAs [17,18]. 6mA has been reported to be enriched in regions of stress-induced DNA double helix destabilization and to regulate the chromatin structure by antagonizing the binding of SATB1 to DNA, thereby affecting early embryonic development [19].

To date, the distribution and function of 6mA in mammalian genomes remain poorly understood. In general, the 6mA level in mammalian cells is extremely low [20,21], and 6mA probably appears only under specific biological conditions or in specific cells [19]. Furthermore, prokaryotic DNA contamination is ubiquitous in the environment, and the 6mA content in prokaryotic genomic DNA is overwhelmingly high; for example, the amount of 6mA in *Escherichia coli* (*E. coli*) genomic DNA ranges from 1.7%–2.7% [21], and the 6mA level is approximately 0.2%–2% in the DNA of mycoplasma (a common microorganism contaminant in laboratory-cultured cells) [22]. This poses challenges for detecting 6mA in eukaryotic DNA. Technically, commercially available antibodies may nonspecifically bind to 6mA-lacking DNA, yielding false positive results [23,24].

Although high-throughput sequencing methods with single-base resolution have been developed for 6mA analysis [25–29], their application to mammalian genomes remains challenging due to the potentially extremely low abundance of 6mA [30,31]. As the gold standard for qualitative and quantitative assessments, ultrahigh-performance liquid chromatography–tandem mass spectrometry (UHPLC–MS/MS) is widely used for the identification and quantification of DNA 6mA [32]. This method involves multiple processes, including sample collection, cell lysis, protein removal, DNA precipitation/adsorption, DNA enzymatic digestion, and UHPLC–MS/MS analysis, all of which could introduce prokaryotic DNA 6mA contamination. To ensure precise terminology throughout this manuscript, we use "6mA" to refer to the biological DNA base modification (N6-methyladenine) and "6mdA" to denote the specific deoxynucleoside analyte (N6-methyl-2'-deoxyadenosine) measured by liquid chromatography (LC)-MS/MS after DNA digestion. In our previous work, we developed a metabolically generated stable isotope labeling method [33], which enabled us to exclude 6mA

contamination introduced by sample pretreatment and the 6mA generated by the coinhabitant mycoplasma during cell culture, allowing the identification of methyltransferase-deposited 6mA in cultured mammalian cells. Additionally, this stable isotopic labeling method can be used to identify phase-delayed 6mA, which is incorporated by DNA polymerase [34–37]. However, heavy stable isotope labeling methods have limitations when analyzing tissue samples and cells that cannot be cultured and passaged, such as human disease-related tissue samples [38], germ cells or early embryos. Therefore, contamination- and stable isotope label-free methods are highly desirable.

In this work, we showed that the 6mdA may be present within the LC flow path, causing overestimation in 6mA content. We focused on how this flow-path related 6mdA contamination can be eliminated by developing a novel migration-retardation separation approach using two tandem LC columns. To ensure the robustness of our method in realistic biological scenarios, we validated it in genomic DNA matrices and applied it to quantify 6mdA across 12 mammalian cell lines. Crucially, direct comparison revealed that conventional single-column methods can overestimate 6mA levels by up to 30-fold due to this hidden interference. By effectively eradicating this systematic bias, our dual-column strategy provides a highly reliable tool for the accurate, ultra-trace quantification of DNA 6mA in mammals.

2. Methods

(1) Chemicals and Reagents

2’-Deoxyadenosine monohydrate (dA, D7400), 2’-Deoxycytidine (dC, D3897), phosphate-buffered saline (PBS, P5493), and ammonium bicarbonate (5330050050) were purchased from Sigma–Aldrich. N6-Methyl-2’-deoxyadenosine (6mdA, sc-222031) was purchased from Santa Cruz. Quick calf intestinal alkaline phosphatase (CIP, M0525S) and RNase A (T3018L) were obtained from New England Biolabs, Dulbecco’s modified Eagle’s medium (DMEM, 11965092), RPMI 1640 medium (11875093), penicillin–streptomycin (15070063) were purchased from Gibco. SuperNuclease (SSNP01) was purchased from Sino Biological. snake venom phosphodiesterase I (SVP, LS003926) was obtained from Worthington. Fetal bovine serum (FBS, 11011-8615) was obtained from Every Green.

To prevent external contamination, certified nuclease-free plastic tubes and pipette tips were used for sample preparation. Glassware and LC solvent bottles were cleaned following standard analytical protocols and thoroughly rinsed with LC-MS grade water. All mobile phases were prepared using standard LC-MS grade solvents.

(2) Cell culture

A549, MCF7, J774, RAW264.7, and SVG p12 cells were cultured in high-glucose DMEM supplemented with 10% FBS and 1× penicillin–streptomycin. K562, Jurkat, NB4, U937, and MOLT-4 cells were cultured in RPMI 1640 medium supplemented with 15% FBS and 1× penicillin–streptomycin. All the cells were incubated in a humidified 37 °C incubator supplied with 5.0% CO_2.

(3) DNA extraction and digestion

Mammalian genomic DNA was extracted with a Wizard Genomic DNA Purification Kit (Promega) following the manufacturer’s instructions with slight modifications. For the cells, the cell pellets were resuspended in 600 μL of nuclear lysis solution. Then, 50 μg of RNase A was added to the lysis mixture and incubated at 37 °C for 0.5 h. Two hundred microliters of protein precipitation solution were added, and the mixture was vortexed for 20 s. The mixture was then centrifuged at 16,000 × g for 10 min at 4 °C,

after which the supernatant was transferred to a clean plastic tube (1.5 mL) filled with 600 µL of isopropanol and centrifuged at 14,000 × g for 2 min at room temperature. After washing twice with 70% ethanol, the DNA pellet was air dried for 3–5 min, and then 50 µL of 10 mM Tris-HCl (pH 8.0) was added to redissolve the DNA. For the tissue samples, 600 µL of lysis buffer supplemented with 10 mM EDTA and 4 U of proteinase K was added to the tissue samples, which were incubated at 55 °C for 5 h to ensure complete digestion. The remaining steps were consistent with those used for the extraction of DNA from cells.

The extracted DNA was digested into 2‘’-deoxyribonucleosides by incubation with a digestion mixture (10 mM Tris-HCl (pH 8.0), 1 mM $MgCl_2$, 1 U of SuperNuclease, 0.02 U of Phosphodiesterase I and 1.0 U of CIP) for 2 h at 37 °C. Ultrafiltration was performed with ultrafiltration tubes (molecular weight cutoff: 3 kDa; Pall Corporation, Port Washington, NY, USA) to remove the enzymes.

(4) UHPLC–MS/MS analysis of dA and dC

UHPLC–MS/MS analysis was performed on an Agilent 1290 Infinity II LC system coupled with an Agilent 6470 triple quadrupole mass spectrometer (Santa Clara, CA, USA). A reversed-phase Agilent Poroshell 120 EC-C18 column (2.1 × 50 mm I.D., 1.9 µm particle size) was used for UHPLC separation. Ultrapure water supplemented with 1 mM NH_4HCO_3 (A) and pure methanol (B) were used as the mobile phases.

The following gradient elution for UHPLC separation was used: 0−2.0 min, 5.0% B, 0.25 mL/min; 2.0−4.0 min, 5.0%−20.0% B, 0.25 mL/min; 4.0−5.0 min, 20.0% B, 0.25 mL/min; 5.0−5.1 min, 20.0%−5.0% B, 0.25−0.3 mL/min; and 5.1−6.5 min, 5.0% B, 0.3 mL/min. The mass spectrometer was operated in positive ion mode with a capillary voltage of 4000 V, temperature of 300 °C and nitrogen as the drying gas operated at 10 L/min; additionally, the fragmentor voltage was 80 V. Multiple reaction monitoring mode was adopted with m/z 252.0→136.0 for dA and m/z 228.0→112.0 for dC, and the collision energy was set to 5 eV.

(5) UHPLC–MS/MS analysis of 6mdA

UHPLC–MS/MS analysis was performed on an Agilent 1290 Infinity II LC system coupled with an Agilent 6495 triple quadrupole mass spectrometer (Santa Clara, CA, USA). A reversed-phase Agilent Zorbax Eclipse Plus C18 column (2.1 × 50 mm I.D., 1.8 µm particle size) was used for separation as the analytical column, and an Agilent Zorbax Eclipse Plus C18 column (4.6 × 50 mm I.D., 1.8 µm particle size) was used as the enrichment column. Ultrapure water supplemented with 1 mM NH_4HCO_3 (A) and pure methanol (B) were used as the mobile phases. The mass spectrometer was operated in positive ion mode, and the parameter settings were as follows: capillary voltage, 4000 V; gas temperature, 150 °C; gas flow, 11 L/min; sheath gas temperature, 350 °C; sheath gas flow, 11 L/min; and nebulizer pressure, 30 psi. Multiple reaction monitoring mode was adopted with m/z 266.0→150.0 for 6mdA, and the collision energy was set to 15 eV.

(6) Method validation

To evaluate the analytical performance and general applicability of the proposed dual-column strategy in realistic biological samples, matrix-matched validation was performed. Three different matrices were evaluated: pure solvent (H_2O), enzymatic digestion mix, and mammalian genomic DNA matrix (2 µg gDNA digest). For the spike-in experiments, 6mdA standards were spiked into the aforementioned matrices to yield a series of final concentrations (0, 2.5, 5, 10, 20, and 100 pM). Each concentration level was analyzed in triplicate (n = 3). The analytical parameters were evaluated as follows:

Precision: The intra-assay precision was expressed as the relative standard deviation (RSD, %) of the peak areas from the triplicate injections.

Matrix effect: The matrix effect was comprehensively evaluated by comparing the slopes of the calibration curves obtained in the respective matrices with that obtained in the pure solvent (H_2O). The matrix effect was calculated using the following equation:

$$\text{Matrix effect (\%)} = (\text{Slope}_{\text{matrix}}/\text{Slope}_{\text{solvent}}) \times 100.$$

Spike recovery: The recovery in the gDNA matrix was calculated by subtracting the endogenous 6mdA peak area (determined from the unspiked 0 pM gDNA sample) from the total peak area of the spiked gDNA sample, and then dividing by the peak area of the corresponding standard in H_2O.

3. Results

3.1. Flow path-related 6mdA contamination in the UHPLC–MS/MS system

To construct a standard curve, a series of 6mdA standards with concentrations ranging from 0–100 pM were analyzed. The standard curve exhibited excellent linearity but did not intersect the origin, suggesting the presence of systematic bias (Figure 1A,B). Consistently, we observed a 6mdA peak upon injection of the 0 pM 6mdA standard (in the absence of 6mdA). Furthermore, we did not observe an increase in the 6mdA peak intensity upon injection of 10.0 µL of the 1.0 pM 6mdA standard. Only after injecting 10.0 µL of the 5.0 pM 6mdA standard did we observe a significant increase in the 6mdA peak intensity (Figure 1B). Overall, we speculated that the UHPLC system was contaminated with 6mdA, which interferes with 6mdA analysis and reduces the sensitivity of the UHPLC–MS/MS assay. To validate the presence of 6mdA contamination in the UHPLC system, we injected varying volumes of water (0–10 µL) and detected a 6mdA peak with a constant intensity upon injection of all volumes (Figure 1C,D). To further pinpoint the exact contamination source, a “no injection mode” experiment was performed. In this mode, the autosampler needle remained completely stationary in the needle seat without moving to engage the sample vial, and no injection valve switching occurred. Although the mobile phase continuously flowed through the needle and needle seat, the persistence of the 6mdA signal under these conditions definitively ruled out sample carryover from the vials or the mechanical action of sample drawing. Based on these results, we concluded that the contamination was continuously introduced by the background flow, originating intrinsically from the mobile phase, pump, or system tubing (Scheme 1).

Although the exact origin of this background interference was not experimentally verified in this study, we hypothesize that the 6mdA contamination in the UHPLC system mobile phase might be related to the minute growth of microbes attached to the inner walls of the tubing. DNA polymers degrade during microbial growth or death, and are partly released as mono 2′-deoxynucleosides and potentially secreted into the aqueous solution. Additionally, the degraded DNA may also exist in the form of long-chain DNA or DNA oligos, which might also contain 6mA. However, these forms of 6mA in the aqueous component of the mobile phase cannot be detected by mass spectrometry because of their poor volatility; thus, they would not affect analysis. Regardless of its precise biological or chemical origin, our dual-column setup effectively isolates and eliminates this interference.

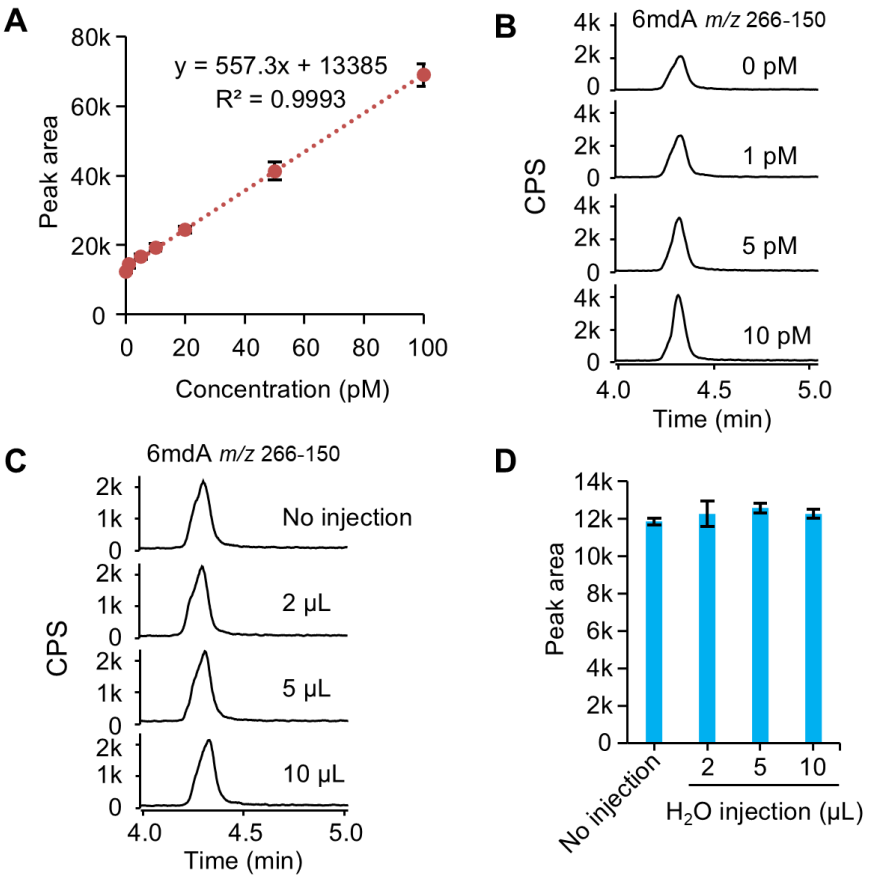

Figure 1. Flow path-related 6mdA contamination in UHPLC-MS/MS system. **(A, B)** Standard curve **(A)** and chromatograms **(B)** for 6mdA were shown with a concentration range of 0–100 pM and only 0–10 pM, respectively; **(C, D)** Chromatograms **(C)** and peak areas **(D)** for water injected at volumes ranging from 0 to10 µL.

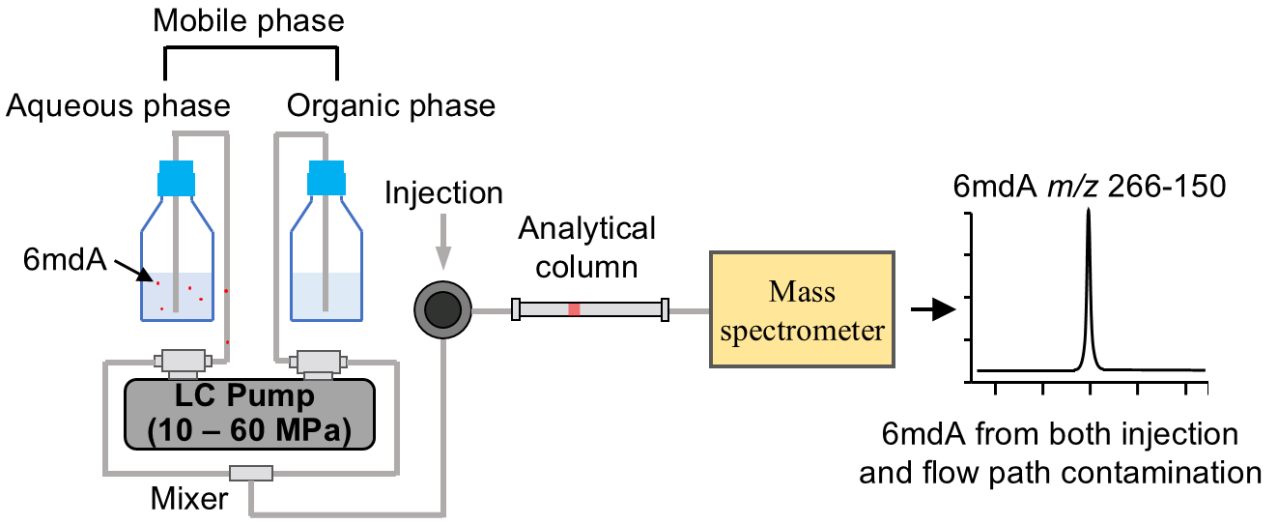

Scheme 1. A schematic diagram illustrating the identification of 6mdA contaminant in UHPLC-MS/MS system.

3.2. Retarded migration-based separation to eliminate interference from 6mdA contamination in the flow path

To eliminate interference from 6mA contamination in the flow path, a cleanup separation method was added for UHPLC–MS/MS analysis (Scheme 2). This was achieved by utilizing two sequentially connected columns. The first column, referred to as the cleanup column, was positioned before the six-way valve of the injector in the UHPLC system. This column captures the UHPLC flow path 6mdA contaminant when the proportion of the organic phase (methanol) is low (methanol:water ratio of 5:95, v/v). This ensures that the mobile phase carrying the sample components through the second (analytical) column is free from flow path 6mdA contamination.

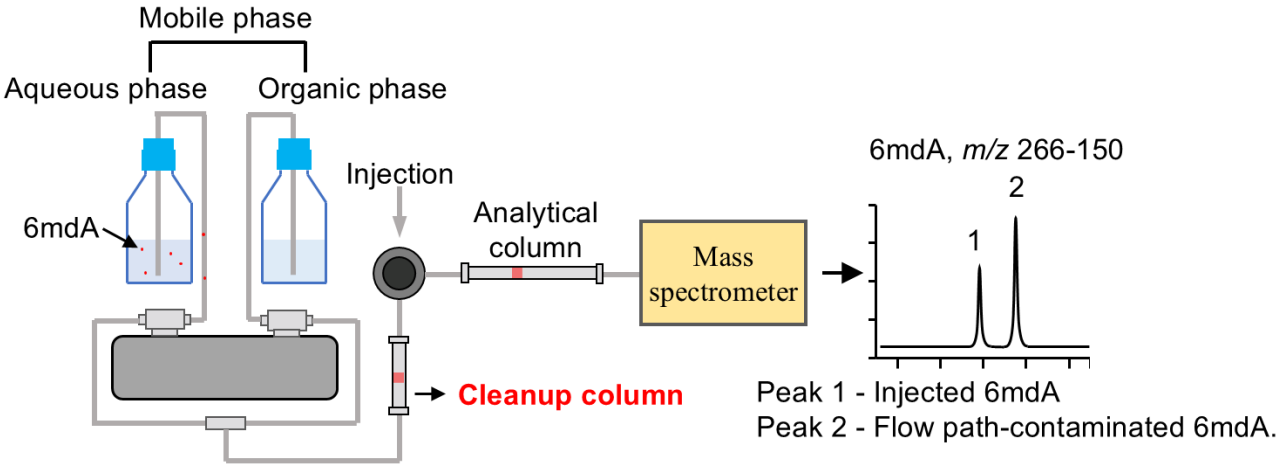

Scheme 2. Schematic diagram of the LC system equipped with an additional cleanup column before the injector's six-way valve, designed to capture flow path-contaminated 6mA. Peak 1—Injected 6mdA; peak 2—Flow path-contaminated 6mdA.

As the proportion of the organic phase increased to elute 6mdA, the 6mdA analyte from the sample passes through the analytical column only and is eluted earlier (Figure 2A, peak 1), whereas the flow path 6mdA contamination from the aqueous component of the mobile phase must pass through both the first (cleanup) and second (analytical) columns, resulting in 6mdA having a longer retention time or retarded migration (Figure 2A, peak 2). This configuration allows for complete resolution of the two 6mdA species (flow path 6mdA and injected sample-containing 6mA). When a 5×10^{-18} mol 6mdA standard (0.5 pM, 10.0 µL) was analyzed, the average signal-to-noise ratio was 11.9, with a relative standard deviation (RSD) of 10.7% (n = 8) (Figure 2 B,C). Thus, this setup enabled the quantification of as few as 3 6mdA molecules per cell when 1 million cells were analyzed (each well of a 6-well plate typically accommodates approximately 1–5 million cells). For human cells, this corresponds to a 6mdA content of approximately 1.7 6mA per 10^9 dA. This is the highest sensitivity achieved to date.

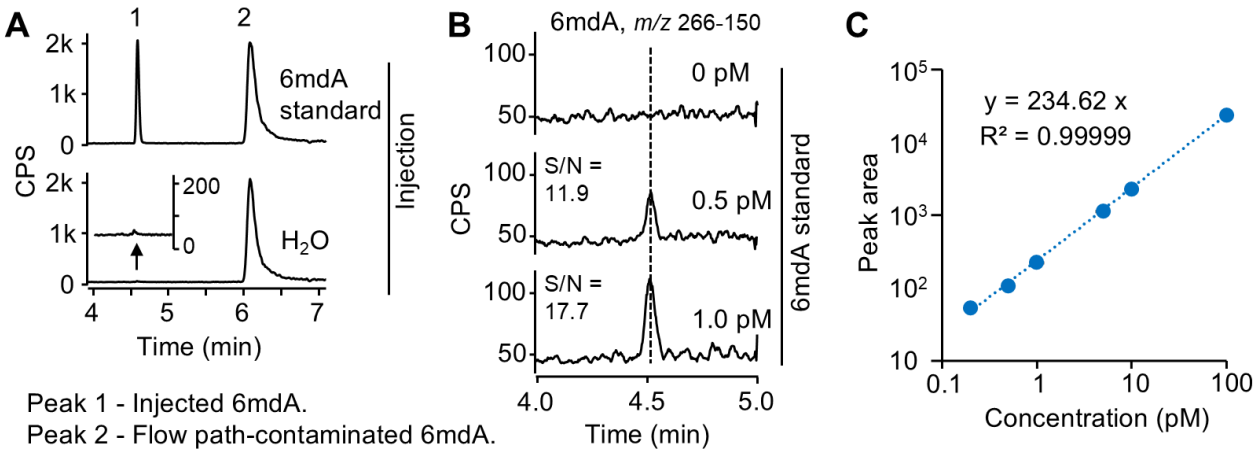

Figure 2. Retarded migration-based separation strategy for resolving flow path-contaminated 6mdA and injected 6mdA from samples. **(A)** Chromatograms illustrating the complete resolution of flow path-contaminated 6mdA and injected 6mA standard; **(B)** Chromatograms of injected 6mdA standards at concentrations of 0, 0.5, and 1.0 pM, showcasing effective elimination of flow path-contaminated 6mdA interferences. S/N–signal-to-noise ratio; **(C)** Standard curve of 6mdA ranging from 0 to 100 pM, obtained using the retarded migration-based separation strategy.

Building upon this exceptional sensitivity, we further systematically validated the analytical performance and robustness of this dual-column strategy across different matrices, including pure solvent (H_2O), enzymatic digestion mix, and authentic complex matrices (2 μg digested mammalian gDNA). As summarized in Table 1, the method exhibited excellent linearity ($R^2 > 0.999$) in all tested matrices. The precision was highly satisfactory, with RSDs ranging from 0.08% to 10.2%. Additionally, the dual-column and valve-switching configuration maintained excellent chromatographic stability, yielding a retention time RSD of 0.35% across 60 consecutive injections. Furthermore, the matrix effects for the enzymatic digestion mix and digested gDNA were evaluated at 95.3% and 100.5%, respectively, indicating negligible matrix interference (ion suppression or enhancement). Notably, the spike recoveries in the digested gDNA matrix ranged from 96.4% to 108.1%. These robust validation results collectively confirm that our method possesses high accuracy, reliability, and excellent applicability for the ultra-trace quantification of 6mdA in authentic biological samples. Overall, these results indicate that our method is accurate and reliable for quantifying 6mdA in biological samples.

Table 1. Analytical performance parameters and method validation for 6mdA quantification in different matrices.

Matrix	Linear Equation	R^2	RSD (%)	Matrix Effect [a] (%)	Spike recovery (%)
H_2O (Solvent)	y = 806.3x	> 0.999	0.08–7.8	-	-
Enzymatic digestion mix	y = 768.3x	> 0.999	0.88–6.5	95.3	-
Digested gDNA (2 μg)	y = 810.0x + 253.9	> 0.999	1.6–10.2	100.5	96.4–108.1

[a] The matrix effect was calculated as the ratio of the calibration curve slope in the specific matrix to that in the H_2O solvent.

3.3. Quantification of nuclear DNA 6mdA in cultured mammalian cells

Prior to analyzing the cellular samples, we evaluated an extraction and digestion blank. As shown in Figure 3A, no detectable 6mdA peak was observed, confirming that no external contamination was introduced during the sample preparation process. Furthermore, to demonstrate the necessity of our dual-column strategy, we compared the 6mdA levels in representative cell lines (MCF7, T47D, and A549) measured by both the conventional single-column method and our proposed method. As summarized in Table 2, the conventional method suffered from severe flow path contamination, leading to an overestimation of endogenous 6mdA levels by approximately 16.1- to 30.4-fold. By effectively eliminating this systematic bias, our method provides a much more accurate assessment. Using this established, reliable, analytical method, we quantified the levels of 6mdA in 12 cell lines (MCF7, T47D, A549, SVG p12, Jurkat, KG-1a, K562, THP-1, U937, MOLT-4, J774, and RAW264.7). The levels of 6mA in 10 of these cell lines were less than 5.0 6mdA per 10^8 dA, whereas the 6mdA levels in 2 mouse macrophage lines, J774 and RAW264.7, were greater, with levels of 1.10 6mdA per 10^6 dA and 1.12 6mdA per 10^6 dA, respectively (Figure 3B–D). The markedly lower levels of 6mdA in most of these cell lines suggest that this modification might be less prevalent or dynamically regulated in certain types of cells under specific conditions. On the other hand, the elevated levels observed in the mouse macrophage cells J774 and RAW264.7 could indicate the potential role of 6mdA in immune-related functions or responses.

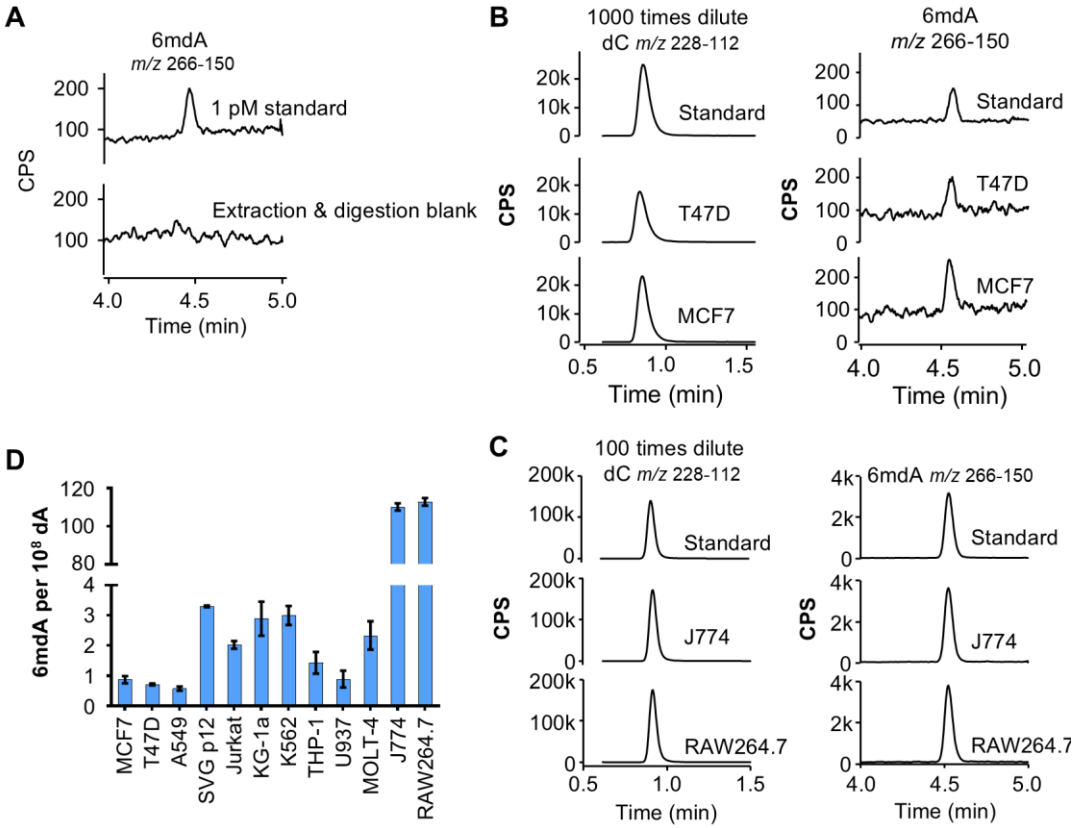

Figure 3. Quantification of nuclear DNA 6mdA in cultured human and mouse cells. **(A)** Chromatogram of 6mdA in extraction & digestion blank; **(C, D)** Chromatograms **(B, C)** and quantification **(D)** of 6mdA of cell lines.

Table 2. Comparison of 6mdA quantification results in representative cell lines using the conventional single-column and proposed dual-column methods.

Cell Line	6mdA level (6mdA per 10^9 dA)		Overestimation Factor [a]
	Conventional single-column method	Proposed dual-column method	
MCF7	140 ± 6.3	8.7 ± 1.2	~ 16.1 ×
T47D	201 ± 12	7.1 ± 0.3	~ 28.3 ×
A549	173 ± 4.9	5.7 ± 0.7	~ 30.4 ×

[a] Overestimation factor is calculated as the ratio of the value obtained by the conventional method to that by the proposed method.

This study identified a previously unrecognized source of contamination in DNA 6mdA analysis originating from the LC flow path itself. This contamination, potentially arising from reagents, solvents, or even the instrument tubing, poses a significant hurdle, particularly when analyzing low-abundance 6mA in mammalian DNA. To address this, we developed a novel flow path 6mdA migration-retardation separation method. This method's strength lies in its ability to physically isolate and eliminate contaminating 6mA during the analysis, ensuring accurate quantification. A key advantage of this retarded-migration strategy is its universal applicability. While rigorous cleaning or fresh mobile phases may temporarily reduce background noise, trace contaminants often fluctuate unpredictably. By physically separating system-derived interferences from the target analyte based on their spatial origins, our dual-column setup ensures reliable results regardless of the system’s contamination severity or tubing conditions, serving as a hardware-level safeguard for routine ultra-trace analysis.

4. Conclusion

We identified 6mA contamination originating from the LC flow path, including the mobile phase and instrument tubing, as a critical hidden interference during LC-MS analysis. To address this, we developed a novel flow path 6mdA migration-retardation separation method. This method effectively separates flow path-related 6mA contamination from sample-derived 6mdA, enabling accurate quantification of 6mdA in biological samples. The limit of quantification for this method was determined to be 5 amol with a signal-to-noise ratio (S/N) ≥ 10. Crucially, through validation and application across 12 mammalian cell lines, we demonstrated that conventional single-column methods can overestimate 6mA levels by up to 30-fold due to this flow-path interference. By thoroughly eliminating this systematic bias and overcoming matrix effects, our strategy enables the ultra-sensitive and accurate quantification of 6mA, providing a highly reliable analytical tool to uncover its true biological functions in mammals.

Declaration of generative AI and AI-assisted technologies

During the preparation of this manuscript, the authors used generative AI tools only to improve language and readability. Specifically, the authors used Gemini for language polishing only in limited sections of the manuscript. The authors take full responsibility for the content of the manuscript.

Acknowledgments

Funding: This work is supported by the National Natural Science Foundation of China (22522412, 22274166 and 22234008), National Key R&D Program of China (2024YFA0918800), and the Strategic Priority Research Program of the Chinese Academy of Sciences (XDB0750100).

Authors' contribution

Conceptualization, H.W. and W.L.; methodology, W.L. and M.L.; validation, J.M. and Z.H.; formal analysis, W.L.; investigation, W.L. and J.M.; resources, H.W.; data curation, W.L.; writing—original draft preparation, W.L.; writing—review and editing, H.W.; supervision, H.W.; funding acquisition, H.W. and W.L. All authors have read and agreed to the published version of the manuscript.

Conflicts of interest

Meiling Lu is an employee of Agilent Technologies. Meiling Lu declares that this affiliation does not influence the design, analysis, interpretation, or presentation of the results reported in this manuscript. Hailin Wang holds the position of Editorial board member for *Life Analysis* and has not peer reviewed or made any editorial decisions for this paper. The other authors declare no relevant conflicts of interest.

References

[1] Dunn DB, Smith JD. Occurrence of a new base in the deoxyribonucleic acid of a strain of bacterium coli. *Nature* 1955, 175:336–337.

[2] Dunn DB, Smith JD. The occurrence of 6-methylaminopurine in deoxyribonucleic acids. *Biochem. J.* 1958, 68(4):627–636.

[3] Zhang G, Huang H, Liu D, Cheng Y, Liu X, *et al*. N6-Methyladenine DNA modification in drosophila. *Cell* 2015, 161(4):893–906.

[4] Fu Y, Luo G, Chen K, Deng X, Yu M, *et al*. N6-methyldeoxyadenosine marks active transcription start sites in Chlamydomonas. *Cell* 2015, 161(4):879–892.

[5] Luo G, Hao Z, Luo L, Shen M, Sparvoli D, *et al*. N6-methyldeoxyadenosine directs nucleosome positioning in tetrahymena DNA. *Genome Biol.* 2018, 19(1):200.

[6] Beh LY, Debelouchina GT, Clay DM, Thompson RE, Lindblad KA, *et al*. Identification of a DNA N6-Adenine methyltransferase complex and its impact on chromatin organization. *Cell* 2019, 177(7):1781–1796.

[7] Labrie SJ, Samson JE, Moineau S. Bacteriophage resistance mechanisms. *Nat. Rev. Microbiol.* 2010, 8(5):317–327.

[8] Shell SS, Prestwich EG, Baek SH, Shah RR, Sassetti CM, *et al*. DNA methylation impacts gene expression and ensures hypoxic survival of mycobacterium tuberculosis. *PLOS Pathog.* 2013, 9(7):e1003419.

[9] Pukkila PJ, Peterson J, Herman G, Modrich P, Meselson M. Effects of high levels of DNA adenine methylation on methyl-directed mismatch repair in Escherichia coli. *Genetics* 1983, 104(4):571–582.

[10] Low DA, Casadesús J. Clocks and switches: bacterial gene regulation by DNA adenine methylation. *Curr. Opin. Microbiol.* 2008, 11(2):106–112.

[11] Boulias K, Greer EL. Means, mechanisms and consequences of adenine methylation in DNA. *Nat. Rev. Genet.* 2022, 23(7):411–428.
[12] Pan B, Ye F, Li T, Wei F, Warren A, *et al*. Potential role of N6-adenine DNA methylation in alternative splicing and endosymbiosis in Paramecium bursaria. *iScience* 2023, 26(5):106676.
[13] Wang Y, Chen X, Sheng Y, Liu Y, Gao S. N6-adenine DNA methylation is associated with the linker DNA of H2A.Z-containing well-positioned nucleosomes in Pol II-transcribed genes in Tetrahymena. *Nucleic Acids Res.* 2017, 45(20):11594–11606.
[14] Kweon S, Chen Y, Moon E, Kvederaviciutė K, Klimasauskas S, *et al.* An adversarial DNA N6-methyladenine-sensor network preserves polycomb silencing. *Mol. Cell* 2019, 74(6):1138–1147.
[15] Hao Z, Wu T, Cui X, Zhu P, Tan C, *et al*. N6-deoxyadenosine methylation in mammalian mitochondrial DNA. *Mol. Cell* 2020, 78(3):382–395.
[16] Ma C, Niu R, Huang T, Shao L, Peng Y, *et al*. N6-methyldeoxyadenine is a transgenerational epigenetic signal for mitochondrial stress adaptation. *Nat. Cell Biol.* 2019, 21(3):319–327.
[17] Zhang M, Yang S, Nelakanti R, Zhao W, Liu G, *et al*. Mammalian ALKBH1 serves as an N6-mA demethylase of unpairing DNA. *Cell Res.* 2020, 30(3):197–210.
[18] Tian L, Liu Y, Chen L, Tang Q, Wu W, *et al*. Structural basis of nucleic acid recognition and 6mA demethylation by human ALKBH1. *Cell Res.* 2020, 30:272–275.
[19] Li Z, Zhao S, Nelakanti RV, Lin K, Wu TP, *et al*. N6-methyladenine in DNA antagonizes SATB1 in early development. *Nature* 2020, 583(7817):625–630.
[20] Schiffers S, Ebert C, Rahimoff R, Kosmatchev O, Steinbacher J, *et al*. Quantitative LC–MS provides no evidence for m6dA or m4dC in the genome of mouse embryonic stem cells and tissues. *Angew. Chem. Int. Edit.* 2017, 56:11268–11271.
[21] O'Brown ZK, Boulias K, Wang J, Wang SY, O'Brown NM, *et al*. Sources of artifact in measurements of 6mA and 4mC abundance in eukaryotic genomic DNA. *BMC Genomics* 2019, 20(1):445.
[22] Razin A, Razin S. Methylated bases in mycoplasmal DNA. *Nucleic Acids Res.* 1980, 8(6):1383–1390.
[23] Douvlataniotis K, Bensberg M, Lentini A, Gylemo B, Nestor CE. No evidence for DNA N6-methyladenine in mammals. *Sci. Adv.* 2020, 6(12):eaay3335.
[24] Lentini A, Lagerwall C, Vikingsson S, Mjoseng HK, Douvlataniotis K, *et al*. A reassessment of DNA-immunoprecipitation-based genomic profiling. *Nat. Methods* 2018, 15(7):499–504.
[25] Feng X, Cui X, Zhang L, Ye C, Wang P, *et al*. Sequencing of N6-methyl-deoxyadenosine at single-base resolution across the mammalian genome. *Mol. Cell* 2024, 84(3):596–610.
[26] Ma C, Li G, Shao W, Min Y, Wang P, *et al*. Single-nucleotide resolution mapping of N6-methyladenine in genomic DNA. *ACS Central Sci.* 2023, 9(9):1799–1809.
[27] Zhang J, Peng Q, Ma C, Wang J, Xiao C, *et al*. 6mA-Sniper: quantifying 6mA sites in eukaryotes at single-nucleotide resolution. *Sci. Adv.* 2023, 9(42):eadh7912.
[28] Shao W, Wu J, Li G, Min Y, Hu Q, *et al*. Quantitative analysis of N6-methyladenine at single-base resolution in mitochondrial DNA of hepatocellular carcinoma by deaminase-mediated sequencing. *Chinese Chem. Lett.* 2024:110747.
[29] Flusberg BA, Webster DR, Lee JH, Travers KJ, Olivares EC, *et al*. Direct detection of DNA methylation during single-molecule, real-time sequencing. *Nat. Methods* 2010, 7(6):461–465.
[30] Feng X, He C. Mammalian DNA N6-methyladenosine: challenges and new insights. *Mol. Cell* 2023, 83(3):343–351.

[31] Kong Y, Cao L, Deikus G, Fan Y, Mead EA, *et al*. Critical assessment of DNA adenine methylation in eukaryotes using quantitative deconvolution. *Science* 2022, 375(6580):515–522.

[32] Shen C, Wang K, Deng X, Chen J. DNA N6-methyldeoxyadenosine in mammals and human disease. *Trends Genet.* 2022, 38(5):454–467.

[33] Liu B, Liu X, Lai W, Wang H. Metabolically generated stable isotope-labeled deoxynucleoside code for tracing DNA N6-methyladenine in human cells. *Anal. Chem.* 2017, 89(11):6202–6209.

[34] Musheev MU, Baumgärtner A, Krebs L, Niehrs C. The origin of genomic N6-methyl-deoxyadenosine in mammalian cells. *Nat. Chem. Biol.* 2020, 16(6):630–634.

[35] Chen S, Lai W, Li Y, Liu Y, Jiang J, *et al*. Aberrant DNA N6-methyladenine incorporation via adenylate kinase 1 is suppressed by ADAL deaminase-dependent 2′-deoxynucleotide pool sanitation. *EMBO J.* 2023, 42(15):EMBJ2023113684.

[36] Chen L, Zhang Z, Chen H, Xi J, Liu X, *et al*. High-precision mapping reveals rare N6-deoxyadenosine methylation in the mammalian genome. *Cell Discovery* 2022, 8(1):138.

[37] Liu X, Lai W, Li Y, Chen S, Liu B, *et al*. N6-methyladenine is incorporated into mammalian genome by DNA polymerase. *Cell Res.* 2021, 31:94–97.

[38] Lyu C, Niu Y, Lai W, Wang Y, Wang Y, *et al*. Rare and misincorporated DNA N6-methyladenine is a hallmark of cytotoxic stresses for selectively stimulating the stemness and proliferation of glioblastoma cells. *Cell Discovery* 2022, 8(1):39.